



# Modelling of a Grade 91 power plant pressurised header weldment under ultra super-critical creep conditions

R. Ragab<sup>a</sup>, J. Parker<sup>b</sup>, M. Li<sup>a,\*\*</sup>, T. Liu<sup>a,\*</sup>, W. Sun<sup>a</sup>

<sup>a</sup> Faculty of Engineering, University of Nottingham, Nottingham, NG7 2RD, UK

<sup>b</sup> Electric Power Research Institute, Charlotte, NC, USA

## ARTICLE INFO

### Keywords:

Creep  
Damage  
Material property  
Modelling  
Pressurised header  
Weldments

## ABSTRACT

This paper is concerned with the creep-damage modelling of a Grade 91 pressurised header, which was observed to undergo in-service cracking in the weldments. A multi-axial creep damage model of Kachanov type, with a single state damage variable, has been implemented into finite element analysis to study the creep damage responses of weldments and the sub-zones i.e. the base metal (BM), weld metal (WM) and heat-affected zone (HAZ). Material properties for each weld constituent were obtained from the results of accelerated creep tests on materials extracted from the header. Predictions of crack initiation were made for sections of the stub to header welds. This analysis was also used to estimate creep failure life of the header weldment under ultra-super-critical conditions. Further, creep crack growth behaviour was predicted based on time-dependent critical damage growth. The predicted damage distributions and failure mode of the cross-weld creep test specimens were in good agreement with the reported experimental observations. The predicted damage distributions and cracking in the header correlate reasonably well with the reported industrial observations.

## 1. Introduction

Pressure vessels are commonly used in power generation industry as part of the system required to provide steam for turbines. With the increasing drive to enhance the thermodynamic efficiency and reduce greenhouse gas emissions, these components are expected to operate under ultra-super-critical conditions (i.e. power plants operate at steam pressure exceeding 20 MPa and operating temperatures higher than 600 °C) [1]. Tempered martensitic steels with 9–12%Cr have been extensively utilized in the construction/retrofitting of power plant header components owing to their excellent properties, e.g., creep strength and oxidation resistance [2]. The current work considers the in-service behaviour of a header which operated at the Aberthaw Power Station, a schematic diagram is shown in Fig. 1 [3,4]. When these headers operate under baseload conditions, the performance of 9–12% Cr welded connections is typically dominated by creep mechanisms. Early in life issues, for example, creep damage or cracking has been found to occur in the heat-affected zone (HAZ) of the welds. This has been commonly referred to as Type IV cracking [3,4]. Without suitable inspection and action cracks at these locations could eventually lead to the failure of components. Therefore, creep performance of 9–12% Cr

steel weldments is a key concern in the assessment of components integrity and lifetime. For this reason, accurate prediction of damage locations, identification of failure mechanism and reliable life assessment of weld in components operating under creep conditions are critical to ensure safe, efficient and reliable power plant operation.

Creep-damage analysis of Grade 91 steel weldments is complicated due to the presence of distinct microstructure regions across the weldment, which requires robust methods of analysis. Several material behaviour models have been developed for creep analysis and creep life predictions. These range from simple approaches like the power law to more advanced models such as continuum damage mechanics (CDM) models [5–9], theta projection method [10] and Robinson's plasticity model [11]. Among these, continuum damage mechanics (CDM) models have gained popularity as they are able to characterize the full creep regime and can be easily incorporated in a finite element (FE) solver to study creep-damage behaviour of weldments [12–15]. Many previous investigations on the creep-damage assessment of weldment in pressurised header components have focused on creep behaviour of weldment fabricated from CrMoV steels. For instance, Hayhurst *et al.* [16] have performed FE-creep damage analysis to predict creep damage and failure life of low ferritic CrMoV steel welded pipes, based on continuum damage mechanics models specifically developed for these grades of

\* Corresponding author.

\*\* Corresponding author.

E-mail addresses: [ming.li@nottingham.ac.uk](mailto:ming.li@nottingham.ac.uk) (M. Li), [Tao.Liu@nottingham.ac.uk](mailto:Tao.Liu@nottingham.ac.uk) (T. Liu).

<https://doi.org/10.1016/j.ijpvp.2021.104389>

Received 20 September 2020; Received in revised form 15 March 2021; Accepted 18 March 2021

Available online 27 March 2021

0308-0161/© 2021 The Authors. Published by Elsevier Ltd. This is an open access article under the CC BY license (<http://creativecommons.org/licenses/by/4.0/>).

Nomenclature			
$\epsilon_{ij}^c$	Creep strain	$k$	Number of creep curves corresponding to different stress levels
$S_{ij}$	Deviatoric stress	$m$	Number of points per curve
$\sigma_e$	von Mises equivalent stress	$\rho_i$	A scaling factor accounting for the time error in the optimization process
$\sigma_1$	Maximum principal stress	CDM	Continuum damage mechanics
$\sigma_r$	Rupture stress	FE	Finite Element
$\omega$	State variable characterising creep damage	CSEF	Creep Strength Enhanced Ferritic Steel
$\dot{\epsilon}_{c, \min}$	Minimum creep rate	BM	Base metal
$t$	Creep time	WM	Weld metal
$t_f$	Creep rupture life	HAZ	Heat-affected zone
A, n, m, B, $\varphi$ , $\chi$	Uniaxial material constants	PT	Partially transformed zone
$\alpha$	Material constant related to multiaxial stress state		

steel. In addition, Mustata *et al.* [17] and Hyde *et al.* [18] have investigated high-temperature fracture behaviour and creep crack growth in low alloy ferritic welded pipes, based on continuum damage constitutive models. Some recent studies have attempted to investigate fracture and damage behaviour of Creep Strength Enhanced Ferritic (CSEF) steel weldment under creep conditions (e.g. Refs. [14,19,20]) or creep-fatigue conditions [21]. These studies have identified that damage and/or cracking tends to concentrate within a specific microstructural region within the weld, referred to as the HAZ. However, there is still little research available in the literature regarding the prediction of creep crack growth in pressurised header welded connections fabricated from Grade 91 steels. In a recent study by Shlyannikov & Tumanov [22], creep damage and fracture in a plane strain biaxiality loaded plate and 3D finite thickness compact tension specimen are investigated by using damage evolution equations. The damage model for the fracture of the process zone is represented using a stress-based formulation [22]. In addition to the stress-based CDMs, creep damage and fracture have also been examined using ductility-based damage models [23,24]. For instance, Cocks and Ashby [23] developed a multi-axial creep ductility-based model based on the cavity growth theory. On the basis of Cock-Ashby model, creep damage and fracture behaviour of 316H steel at 550 °C have been investigated [25]. Shlyannikov, V. and Tumanov, A. [26] presented an approach to determine creep fracture properties and crack growth behaviour in pure modes I and II using stress-and ductility-based formulations. Based on the ductility model, new multi-axial failure strain conditions are derived [26].

For the purpose of FE creep modelling of the weldments and to account for material heterogeneity, it is often considered that a pipe

weldment constitutes several distinct material zones. Each may have different material properties which are usually determined from creep tests to provide solutions for the material constitutive equations. For instance, novel approaches for determination of the creep constitutive parameters of the base metal (BM), weld metal (WM) and HAZ have been proposed by Hyde *et al.* [13,14,27], based on continuum damage mechanic modelling and utilizing creep tests. In more details, material constants for the base metal and weld metal were identified from a set of uniaxial creep tests and notched bar rupture tests (e.g. Ref. [13]), while the creep properties of the HAZ were derived from cross-weld creep tests and other novel non-standard tests such as impression creep test (e.g. Ref. [14]). Saber *et al.* [28] have proposed a two-material model accounting only for the base metal and weld metal to investigate creep-damage properties of P92 weldment, based on steady-state and creep damage analyses and utilizing accelerated uniaxial and notched bar creep tests, without considering the creep response of the heat-affected zone. As such, creep damage assessments accounting for the three weld constituents (base metal, heat-affected zone and weld metal) are required to investigate the potential creep performance of CSEF steels under ultra-super-critical conditions in future power plant applications.

This paper investigates creep-damage behaviour of a Grade 91 pressurised header under ultra-super critical conditions using CDMs. To achieve this, a multi-axial creep damage model of Kachanov type, with a single state damage variable, is adopted to characterize the material behaviour of weldment under creep conditions. A multi-material model consisting of the BM, WM and the HAZ is utilized to characterize the localized stress-strain distributions and evolution during creep loading.

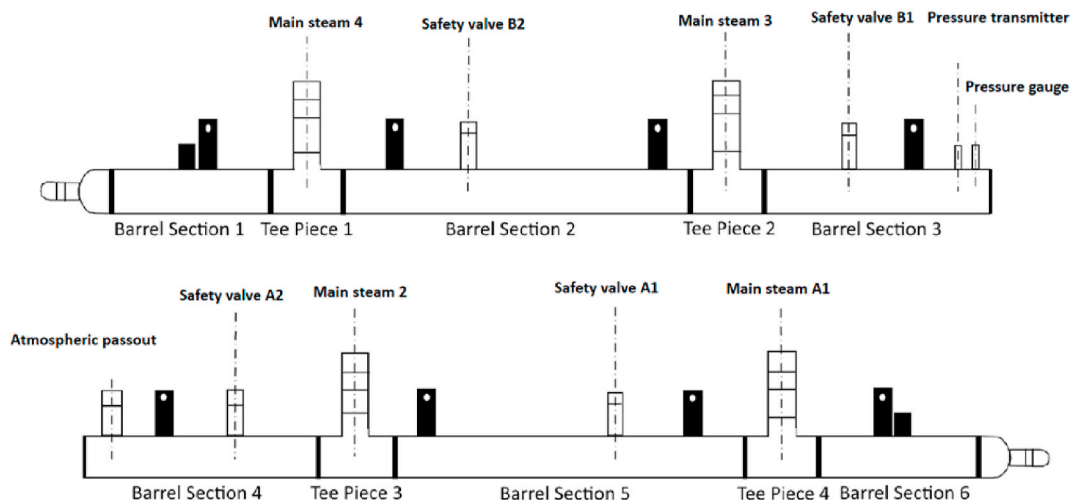


Fig. 1. A schematic diagram showing the general layout of the secondary superheater header which operated at Aberthaw Power Station [3,4].

Material properties for each weld constituent are obtained from creep tests conducted at 625 °C on materials extracted from the ex-service header. Following the determination of creep dependent properties, a 3D FE analysis was performed on the pressurised stubs-header, with the aim to predict the nucleation and evolution of creep damage and to estimate the creep life of these weldments (under ultra-super critical conditions) using ABAQUS FE software package [29]. Moreover, creep crack growth behaviour of the header was predicted using damage mechanics-based material models.

**2. Experimental work**

Creep specimens machined from the ex-service header were tested at a temperature of 625 °C and a specific stress range to investigate the creep response of P91 weldment under both uniaxial and multiaxial stress conditions and to determine specific material constants in the coupled creep-damage constitutive equations introduced in Section 3. The experimental program was conducted following EPRI guidelines and ASTM standard methods, e.g., ASTM E2714-09. The dimensions of the specimens used in the creep and rupture tests (Fig. 2) are chosen for practical reasons (e.g., to enable laboratory metallographic assessment on the tested specimens) and to produce creep fracture behaviour close to that in service. This section presents a summary of the results obtained from creep tests. Further details regarding the experimental work are provided in the cited reference [30,36].

*2.1. Uniaxial creep tests and notched bar creep rupture tests*

Seven uniaxial creep tests were performed to obtain the uniaxial creep strain and creep rupture data for the P91 BM and the simulated HAZ. The dimensions of the uniaxial specimen used in these tests are

shown schematically in Fig. 2a. The uniaxial tests were performed at 625 °C and under a stress range of 70–120 MPa for the BM, while the simulated HAZ was tested under a stress range of 45–80 MPa. The simulated HAZ terminology in the present study refers to a specific weld region generated from the application of simulated welding thermal cycles to replicate the mechanical and microstructural properties of the “real” HAZ [34,35]. To study the creep response of materials under multi-axial loading conditions, six notched bar creep rupture tests were performed at 625 °C and under a nominal stress (on the minimum notched cross section) range of 100–160 MPa for the BM and 60–100 MPa for the simulated HAZ. The dimensions of the notched bar specimen are shown in Fig. 2b. The failure times of the uniaxial creep tests and

**Table 1**

Summary of smooth bar and notched bar creep rupture tests for the P91 BM and HAZ [30,36].

Material	Test	Temperature (°C)	Stress (MPa)	Rupture time (hours)
BM	Plain Bar	625	70	13603*
			80	7291.5
			100	994.2
			120	142.1
			120	8272.8
HAZ	Plain Bar	625	45	17873.4*
			60	3144.8
			80	365.8
			60	14836.1
			80	1938.0
HAZ	Notched Bar	625	100	759.0
			120	3349.3
			160	435.9

Nb: The (\*) notation indicates ongoing test.

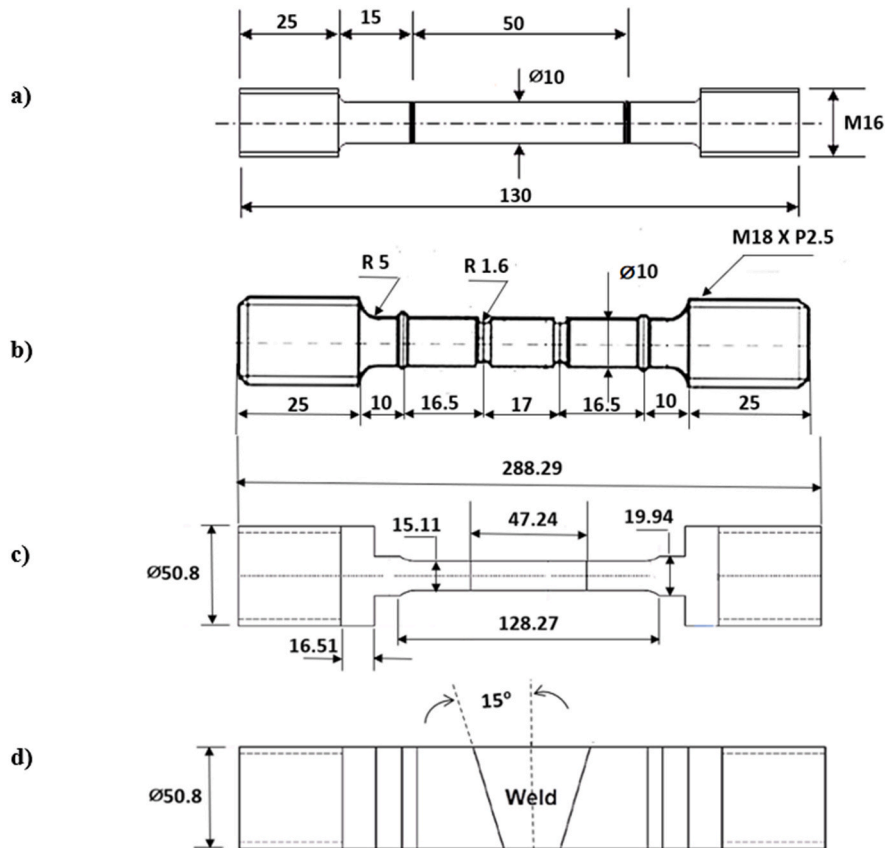


**Fig. 2.** A schematic diagram showing the geometrical details of a) Uniaxial specimen, b) Notched bar specimen, c) Cross-weld specimen (elevation view), and d) Cross-weld specimen (plan view) (All dimensions in mm).

notched bar creep rupture tests are summarized in Table 1. The experimental uniaxial creep curves for the BM and the HAZ are shown in Fig. 3a for a stress level of 80 MPa.

## 2.2. Cross-weld creep tests

Two cross-weld specimens were machined from the P91 weldment, consisting of three different materials; BM, WM and HAZ, to study the mechanical response of this weldment under creep conditions. The geometrical details of the cross-weld specimen are shown in Fig. 2c. The specimen geometries were chosen to induce a multi-axial stress state in the gauge section and therefore to better replicate in-service damage. The cross-weld creep tests were performed at 625 °C and under two nominal stress (on the cross section of the uniform section) levels of 60 MPa and 80 MPa. The experimental results related to these tests are summarized in Table 2 and the creep curves are plotted in Fig. 3b. Further details regarding the experimental work on the cross-weld creep tests are provided in the cited reference [30].

## 3. Determination of the creep properties of the P91 weldment

### 3.1. Creep damage constitutive equations

An empirical creep damage model of Kachanov type has been adopted in this work to characterize the material behaviour of weldment under creep conditions due to its simplicity and computational convenience. The model incorporates one state variable representing material damage, with a value ranges from 0 to 1, corresponding to no damage state and full damage state, respectively. This model has been successfully applied to investigate creep and damage behaviour of power plant steel weldments by Refs. [19,20]. The constitutive equations in the multi-axial form are expressed as follows [5,33]:

For creep strain rate:

$$\frac{d\varepsilon_{ij}^c}{dt} = \frac{3}{2} A \left( \frac{\sigma_{eq}}{1-\omega} \right)^n \frac{S_{ij}}{\sigma_{eq}} t^m \quad (1)$$

For creep damage rate:

$$\frac{d\omega}{dt} = B \frac{\sigma_r^\chi}{(1-\omega)^\varphi} t^m \quad (2)$$

**Table 2**  
Summary of cross-weld creep tests [30].

ID	Temperature (°C)	Stress (MPa)	Rupture time (hours)	Failure location
Test-1	625	60	13201	HAZ
Test-2	625	80	3743	HAZ

where  $S_{ij}$  and  $\varepsilon_{ij}^c$ , ( $i, j = 1, 2, 3$ ) are the deviatoric stress and creep strain components, respectively;  $\sigma_{eq}$ ,  $\sigma_1$  and  $\sigma_r$  are the equivalent, maximum principal and rupture stresses, respectively;  $\omega$  is a state variable characterising creep damage due to internal cavitation,  $\omega \in [0, 1]$ ;  $A$ ,  $n$ ,  $m$ ,  $B$ ,  $\varphi$ ,  $\chi$  are the material constants obtained via uniaxial tensile creep tests. The multi-axiality in this model is accounted for through the rupture stress, and it is assumed to be a combination of the maximum principal stress and von-mises equivalent stress as given below:

$$\sigma_r = \alpha \sigma_1 + (1 - \alpha) \sigma_{eq} \quad (3)$$

where  $\alpha$  is the constant that is related to the material behaviour in the multi-axial stress states. Microstructural investigations conducted by Refs. [30,31] on Grade 91 steel weldment have revealed that creep damage is dominated by cavitation, which is consistent with the model hypothesis regarding the nature of creep damage.

### 3.2. Determination of creep properties of weldments

In order to solve the above constitutive equations, the material constants for each material must be determined first. For this purpose, a multi-material model consisting of the BM, the WM and the HAZ, is used to characterize the localized stress-strain state distribution and evolution during creep loading. For both the BM and HAZ, the six uniaxial constants are determined from the uniaxial creep tests on plain bars, while the triaxial parameter is determined by matching the FE simulation results of the notched bar creep rupture tests with the corresponding experimental results. The creep properties of the WM are determined by comparing FE predictions of cross-weld creep responses with the experimental results. The creep properties obtained for the P91 steel weldment are listed in Table 3.

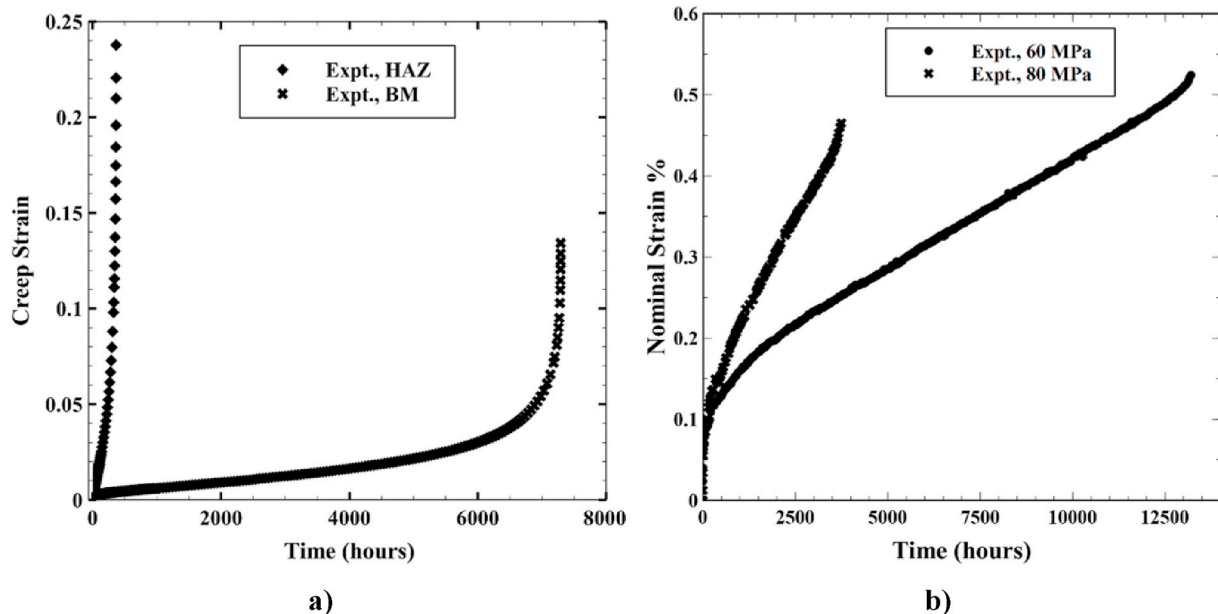


**Fig. 3.** Experimental creep curves at 625 °C for: a) the BM and HAZ under stress level of 80 MPa at 625 °C, and b) the cross-weld specimens.

**Table 3**

Material constants of Kachanov damage model obtained for the P91 BM, WM and HAZ at 625 °C (stresses in MPa, and times in hours).

	A	n	φ	B	χ	m	α
BM	$3.52 \times 10^{-28}$	11.46	10.1	$9.03 \times 10^{-22}$	8.49	$3.8 \times 10^{-3}$	0.18
HAZ	$4.24 \times 10^{-15}$	5.4	3.0	$6.7 \times 10^{-14}$	5.05	0	0.29
WM	$3.0 \times 10^{-28}$	11.33	6.67	$1.2 \times 10^{-21}$	8.54	$9.3 \times 10^{-4}$	0.2

**3.2.1. Determination of uniaxial material constants**

The uniaxial constants (A, n, m, B, φ, χ) for both the BM and HAZ of P91 steel are determined based on the plain bar creep tests performed at different stress levels, following an inverse optimization procedure. First, the multiaxial form of the constitutive equations (1)–(3) is reduced to a uniaxial form by noting that in a uniaxial loading condition the rupture stress, maximum principal stress and von Mises equivalent stress are all equal, and hence yielding the following equations:

$$\frac{d\epsilon^c}{dt} = A \left( \frac{\sigma}{1-\omega} \right)^n t^m \tag{4}$$

$$\frac{d\omega}{dt} = B \frac{\sigma^\chi}{(1-\omega)^\varphi} t^m \tag{5}$$

Integrating equations (4) and (5) with respect to time yields an expression for the uniaxial strain in terms of stress and time as follow:

$$\epsilon^c = \frac{A\sigma^{n-\chi}}{B(\varphi+1-n)} \left[ 1 - \left( 1 - \frac{B(\varphi+1)\sigma^\chi t^{m+1}}{m+1} \right)^{1-\frac{n}{\varphi+1}} \right] \tag{6}$$

The optimization procedure requires initial estimates of the material parameters to be determined. For this purpose, the primary creep is neglected, and the damage is assumed to accumulate in the tertiary creep only (i.e. m = 0). As such, the expression in (4) can be further simplified to Norton’s law, which can be linearized as follow:

$$\log(\dot{\epsilon}_{c, min}) = n \log(\sigma) + \log(A) \tag{7}$$

Similarly, the relationship between the rupture time,  $t_f$ , and the stress,  $\sigma$ , can be expressed as follow:

$$t_f = \frac{1}{B(\varphi+1)\sigma^\chi} \tag{8}$$

$$\log(t_f) = -\chi \log(\sigma) + \log\left(\frac{1}{B(\varphi+1)}\right) \tag{9}$$

The experimental and fitted uniaxial creep and rupture data for the BM and HAZ are shown in Fig. 4a and 4b.

Finally, a group of experimental creep curves were fitted to the uniaxial creep strain curves using equation (6) to determine the material parameters through an optimization technique with the objective function taking the following form [13,15]:

$$\sum_{i=1}^k \left\{ \left[ \sum_{j=1}^m (\epsilon_j^{pred} - \epsilon_j^{exp})^2 \right] + \rho_i \left( \frac{t_{fi}^{pred} - t_{fi}^{exp}}{t_{fi}^{exp}} \right) \right\} \rightarrow \min \tag{10}$$

where k denotes the number of creep curves corresponding to different stress levels; m the number of points per curve;  $\rho_i$  a scaling factor accounting for the time error in the optimization process and its value ranges from 0 to 1; superscript *pred* denotes the quantities from predictions and superscript *exp* denotes the quantities measured from experiments.

The objective function in (10) is solved using MATLAB and the six uniaxial material parameters are determined for both the BM and HAZ as listed in Table 3 and depicted in Fig. 5a and 5b.

**3.2.2. Determination of the multi-axial material parameter, α**

The triaxial parameter was determined by comparing the rupture lives obtained from FE simulations of notched bar creep rupture tests with the experimental times to failure. The values of this parameter spanned a range from zero, where the failure is dominated by von Mises equivalent stress, to unity, where the failure is dominated by the maximum principal stress. Given this range, different values of α are assumed and the corresponding failure times of the notched bars are obtained from the FE damage analysis using all the other material properties already determined from uniaxial data. The analysis has been performed in conjunction with a user defined material model representing Kachanov type model, as given by equations (1)–(3). For the

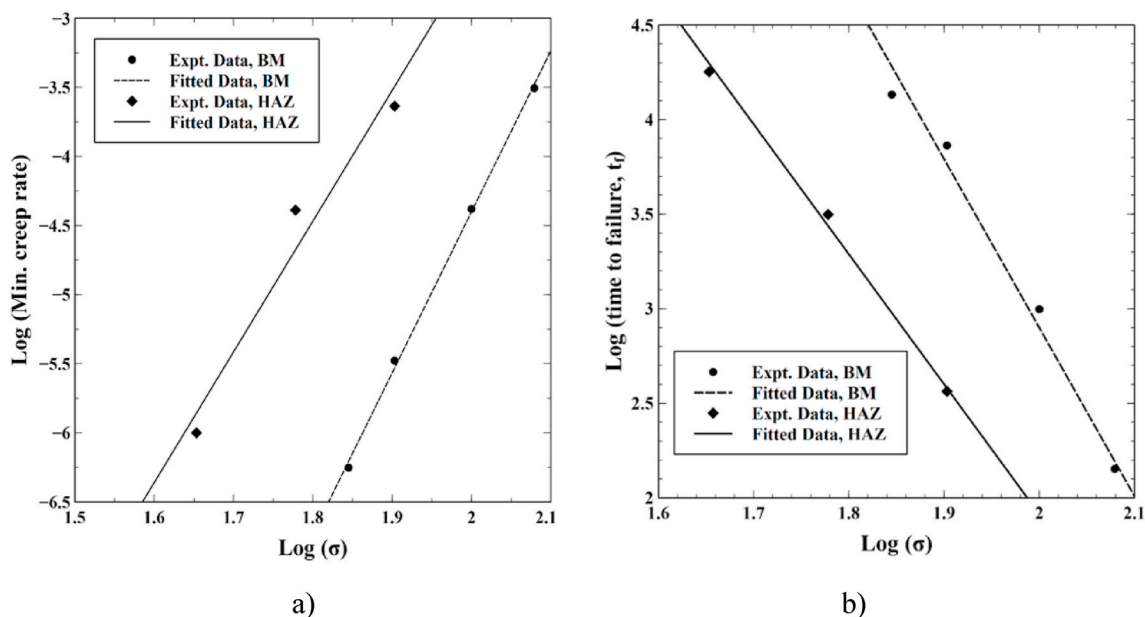


**Fig. 4.** a) Linear correlation between the steady state creep rate and stress, both on logarithmic scales, for the P91 BM and HAZ at 625 °C, and b) Linear correlation between the times to failure and stress, both on logarithmic scales, for the P91 BM and HAZ at 625 °C.

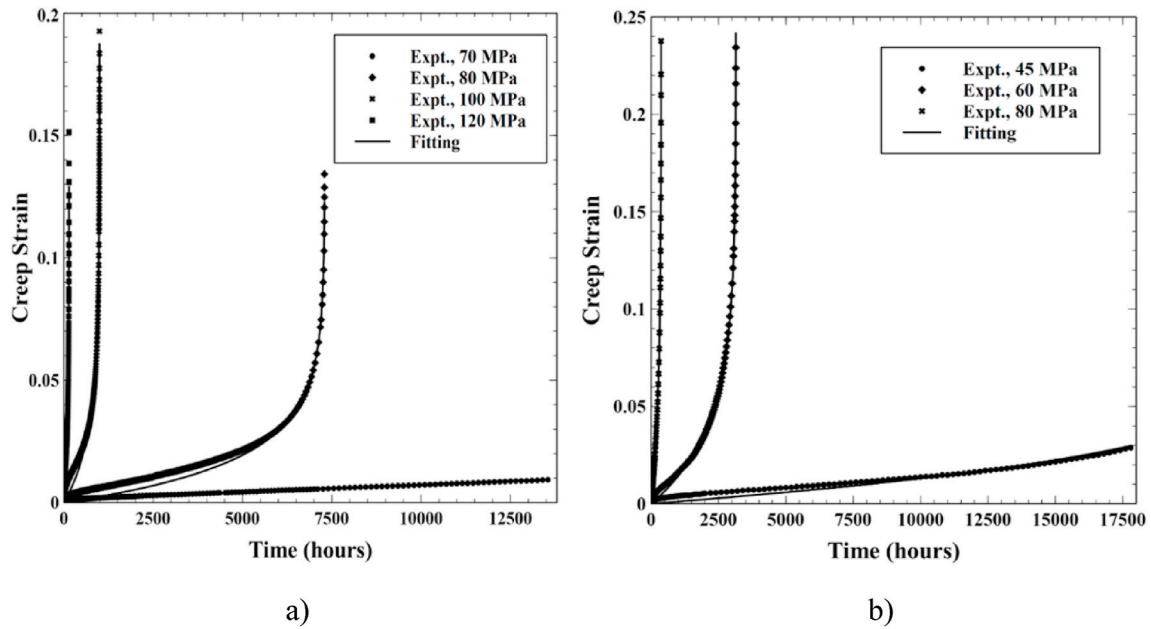


Fig. 5. Experimental and predicted uniaxial creep curves using Kachanov model for: a) the P91 BM (at 625 °C; stress range 70–120 MPa) and b) the P91 HAZ using Kachanov model (at 625 °C; stress range 45–80 MPa).

purpose of FE modelling, the notched bar is modelled using axisymmetric elements with reduced integrations, designated as (CAX8R) in the FE software ABAQUS. The mesh has been refined at the two notches, where stresses are expected to vary rapidly, to obtain more accurate results of the damage variable, as illustrated in Fig. 6. As the FE results are mesh dependent, a prior mesh convergence study was conducted using the maximum von Mises equivalent stress as an indicator, from which the total number of elements were found to be 1024, resulting in negligible stress variation relative to the chosen mesh.

The relationships between the notched bar times to failure and the multi-axial parameter,  $\alpha$ , obtained from creep tests and FE damage analysis, are depicted in Fig. 7a and 7b for the BM and HAZ, respectively.

### 3.2.3. Determination of weld material constants

A multi-material FE damage analysis has been conducted in this section to identify the weld material constants. The creep properties of the WM are determined by comparing the FE predictions of cross-weld

creep response with the experimental results. The identified creep constitutive parameters, listed in Table 3, are used in the multiaxial creep damage model of the cross-weld specimen, which is modelled using 3D quadratic continuum elements with reduced integrations (C3D20R). Taking advantage of the symmetry, only a quarter of the geometry was modelled in ABAQUS, utilizing plane symmetry boundary conditions as illustrated in Fig. 8. The mesh assigned for the cross-weld specimen is shown in Fig. 8, with a local mesh refinement applied at the weld interface regions where stresses are expected to change rapidly. Again, a mesh sensitivity study was performed, using the maximum von Mises equivalent stress as an indicator, from which the total number of elements was found to be 28,000, resulting in negligible stress variation relative to the chosen mesh.

The predicted creep responses of the cross-weld specimen under different stress levels of 60 MPa and 80 MPa and at a temperature of 625 °C are compared with the experimental data, as shown in Fig. 9. Here, the nominal strain was calculated by dividing the gauge length extension at a given time by the initial gauge length. Creep damage

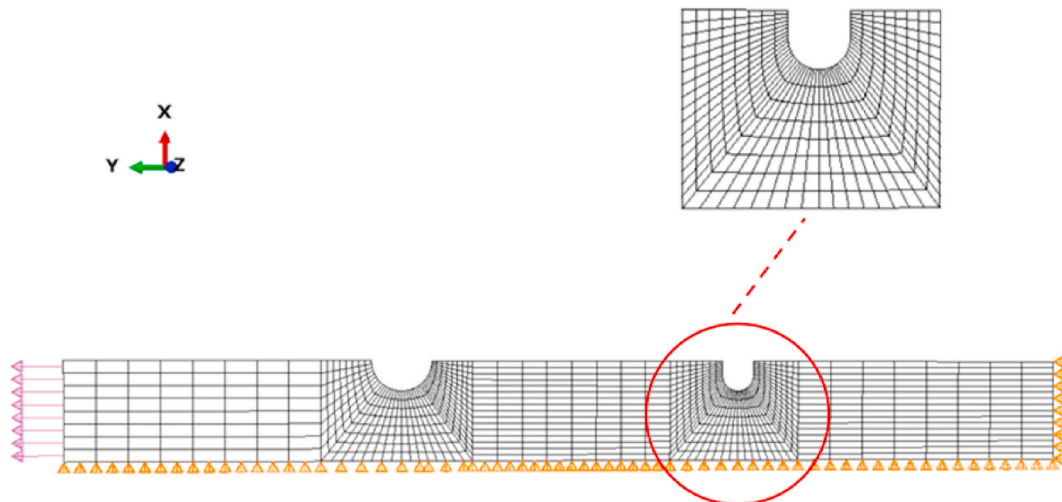


Fig. 6. Notched bar FE model to identify the loading, boundary conditions and mesh scheme.

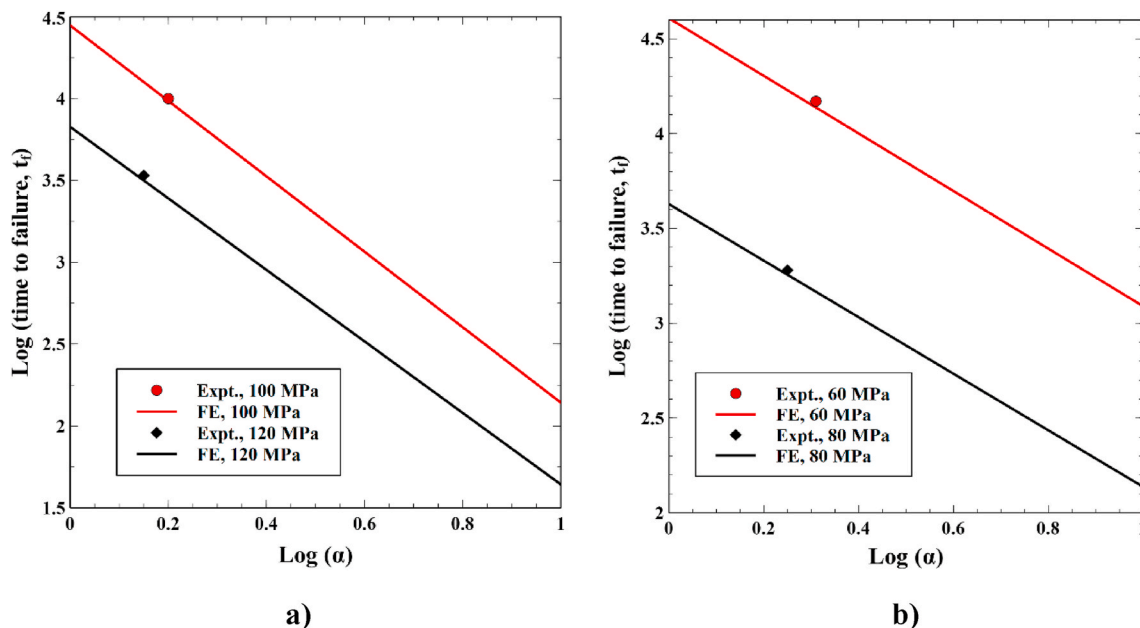


Fig. 7. Determination of the multi-axial parameter,  $\alpha$ , for the P91 BM (average  $\alpha = 0.18$ ) and b) Determination of the multi-axial parameter,  $\alpha$ , for the P91 HAZ (average  $\alpha = 0.29$ ).

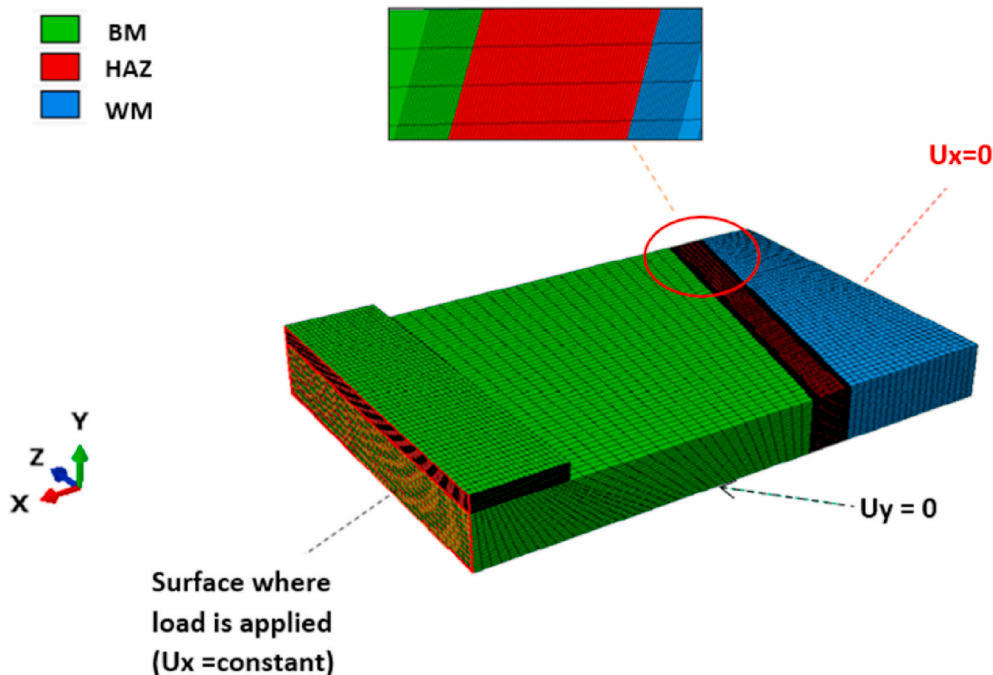


Fig. 8. FE model of the cross-weld creep test specimen.

distributions at a time close to failure are predicted for the cross-weld specimen tested under a stress level of 60 MPa and the results are shown in Fig. 10, which clearly indicate that creep damage is concentrated in the HAZ, with higher damage values predicted in a specific microstructural region in the HAZ, referred to as the partially transformed (PT) zone, as shown in Fig. 10. Similar results were obtained for the cross-weld specimen tested under a stress level of 80 MPa. These predictions agree well with the experimental results of cavitation damage distribution in the cross-weld specimens reported in the cited reference [25]. The FE damage analysis has shown that creep failure occurs in the HAZ, as shown in Fig. 10. These predictions are consistent

with the experimental observations shown in Fig. 10. Table 4 compares the exact macro-failure location within the HAZ as predicted by the FE simulation to that observed in the cross-weld creep tests. It should be noted that the failure location was measured as the distance relative to the fusion line. As illustrated in Table 4, both the FE predictions and the experimental findings are in good agreement.

#### 4. Creep damage analysis of the pressurised header

The weld sections considered in this investigation are stub tubes to Barrel section-2 weldments, as shown in Fig. 1. This selection was made

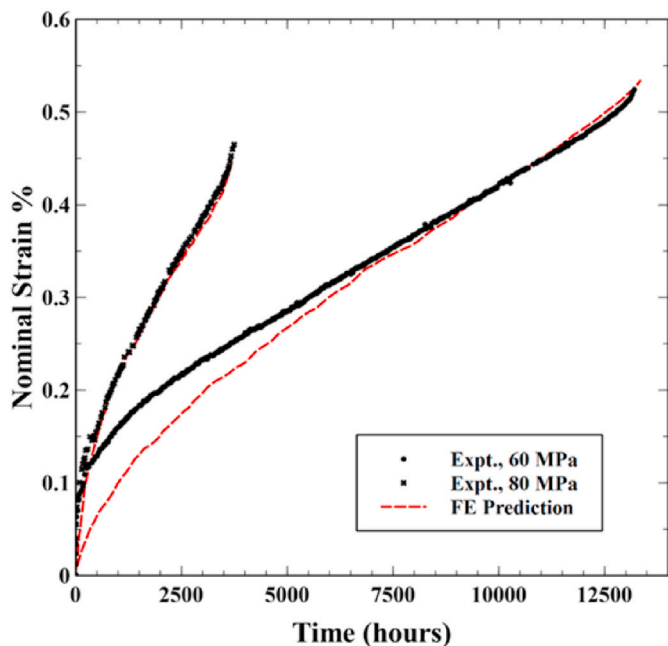


Fig. 9. Experimental and predicted nominal creep strain of the P91 cross-weld specimens at 625 °C.

because these welded connections were shown to undergo significant creep damage during the header service life. The key geometrical details of the analysed sections are illustrated in Fig. 11a. The header has a cylindrical cross-section (450 mm OD x 50 mm WT) referred to as “barrels”, ASTM A335 P91. The stub tubes (54 mm OD x 8 mm WT) are welded to the header barrel section with arrangement mostly at 50° intervals around the circumference between 55° and 305° from the top dead centre position [32]. It should be noted that the header component was analysed under ultra-super-critical ‘temperature’ conditions (i.e., at temperature of 625 °C), which is higher than the industrially recorded operating temperature (570 °C), and under nominal steam pressure of 16.5 MPa to investigate the potential creep-damage of the pressurised header in future power plant applications.

4.1. 3D finite element model

A FE creep damage analysis was performed under an internal pressure of 16.5 MPa using creep continuum damage model, given by equations (1)–(3), with the material properties obtained at 625 °C. The weldment is modelled using three material phases, namely the BM, WM and HAZ as shown schematically in Fig. 11a. Material properties used in the damage calculations are listed in Table 3. The regions of interest were modelled using 3D quadratic continuum elements. Quadratic elements were chosen over elements with linear interpolation function since they better fit the curved geometry and are less susceptible to shear locking in the anticipated bending deformation [29]. Since the FE results are mesh dependent, a prior mesh convergence study was performed, using the maximum equivalent stress as an indicator, from which the total number of elements used in modelling stub tubes weld were found to be 32,749. A negligible stress difference (less than 0.1%) was found relative to the chosen mesh, shown in Fig. 11b. A local mesh refinement was applied to the weld region, where material discontinuity exists. To reduce the computational efforts in terms of analysis time and memory storage, only a quarter of the geometry was modelled in ABAQUS, utilizing appropriate axisymmetric boundary conditions as shown in Fig. 11b. An equation type constraint was also prescribed to the end of the vessel, as shown in Fig. 11b, to maintain planar motion [29]. An internal pressure of 16.5 MPa was applied to the inner surfaces while a proportion of this load was applied as an axial thrust to the end of the vessel and stub tubes. At the end of the stubs, displacements are constant.

Table 4

Comparison between the experimentally observed and the predicted failure locations in the cross-weld test specimens.

ID	Stress level (MPa)	Macro-failure location in the HAZ based on experimental observations (mm) [30]	Macro-failure location based on FE simulation (mm)
Test-1	60	1.625	1.4
Test-2	80	1.440	1.3

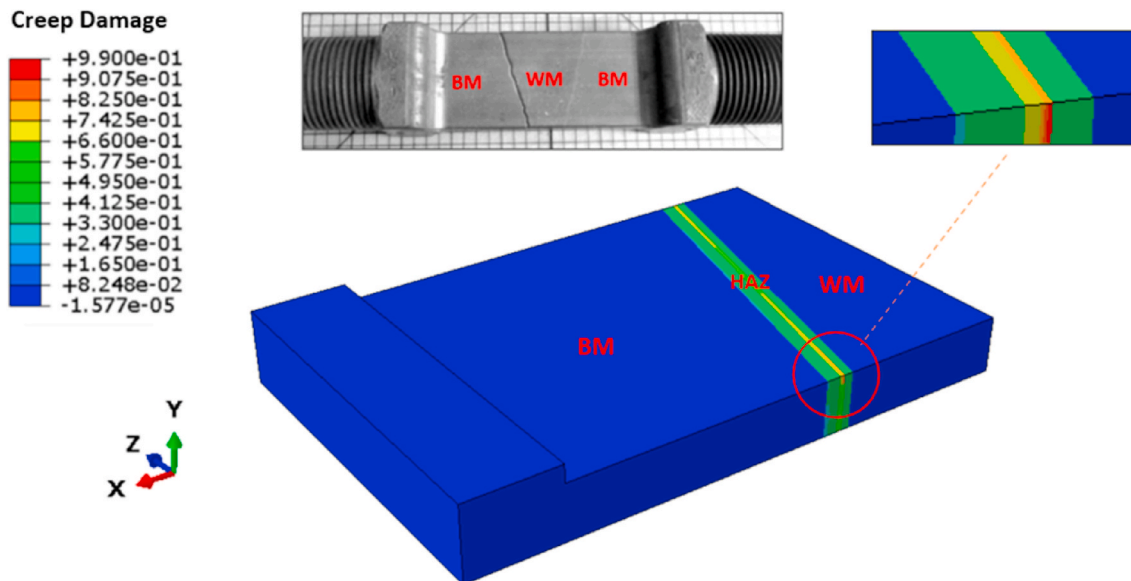
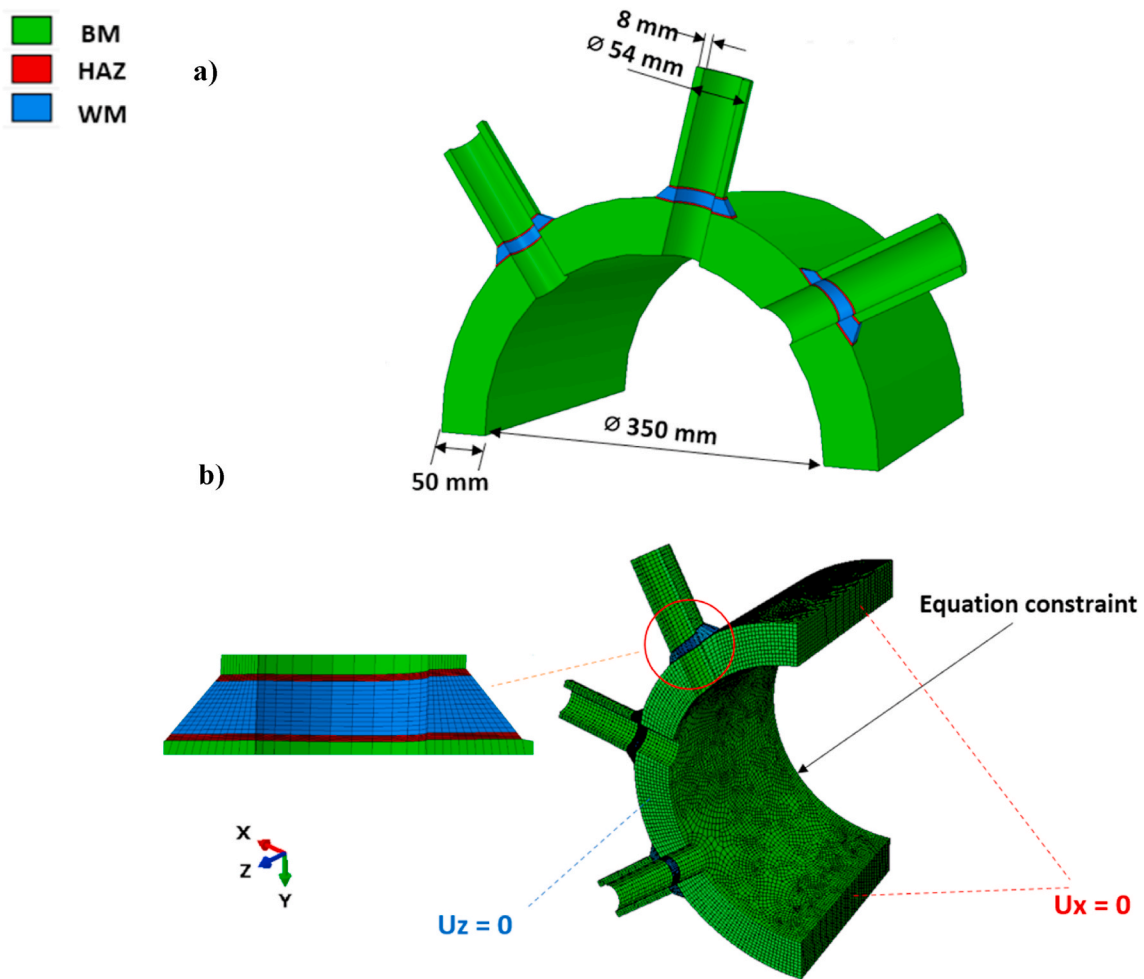


Fig. 10. Predicted creep damage distribution for cross-weld specimen at a time close to failure (at 625 °C and stress of 60 MPa) as compared to the experimentally observed failure mode observed by Ref. [25].



**Fig. 11.** A schematic of the stubs-header model showing a) Geometrical details of the analysed section, and b) Mesh scheme and boundary conditions in the FE model of the stub tube-header weld.

#### 4.2. Continuum damage mechanics analysis of the header

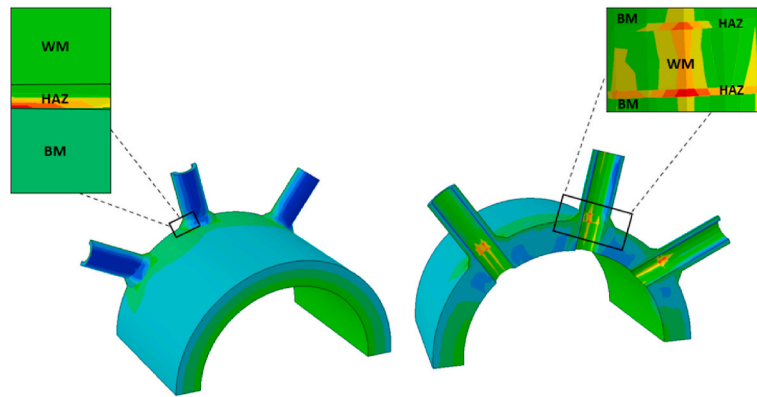
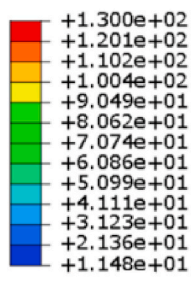
Continuum damage mechanics (CDM) based FE analyses have been performed to estimate the initiation and growth of cracking in the stubs-header weld under ultra-super-critical creep conditions. In the FE damage calculations, material failure at a point is assumed to occur when the damage variable ( $\omega$ ) approaches unity. In the analysis, creep crack initiation is defined as the first element reaching a damage level ( $\omega \approx 1$ ). Once the element has failed, it is assumed incapable of supporting any additional loads, and its elastic modulus is adjusted accordingly to  $\sim$  zero. Creep crack growth is, therefore, simulated by the accumulation of damaged elements with time along the HAZ near the BM.

Fig. 12 shows the predicted von Mises equivalent stress distributions on stubs-header weldment at different times. It should be noted that in Fig. 12a–c, the magnified sections on the left show the distribution of stresses on the outer surface of the stub tubes-header weld, while those on the right show stress distributions on the inner surface of the header. It can be seen that at creep time ( $t$ ) of 300 h, Fig. 12a, stress values tend to peak in the HAZ, adjacent to the BM, where creep cracking is predicted to initiate. When material failure occurs in local material points (elements reaching a damage level,  $\omega \approx 1.0$ ) in the HAZ, stresses are off loaded from the damaged elements and redistributed to adjacent elements due to the increasing creep strain rate during creep process. This

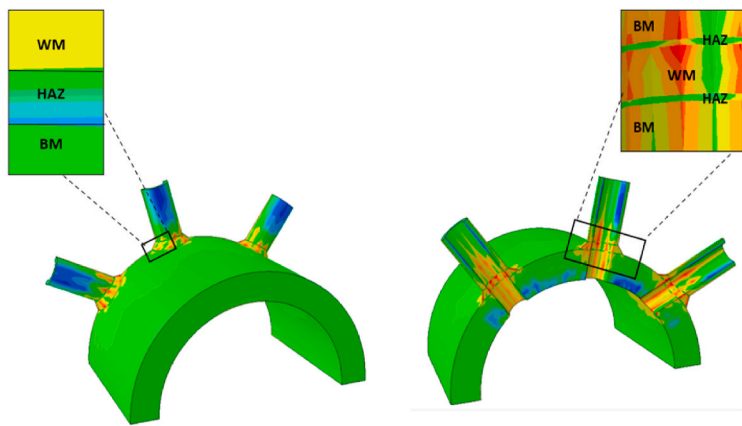
redistribution leads to the enhancement of stresses locally in the BM and the WM, as shown in Fig. 12b and c.

The predicted creep damage distributions for the stubs-header weld connection at different times are presented in Fig. 13a and 13b. These results clearly indicate that creep damage levels in the HAZ are significantly higher than those in the BM and the WM, at all creep times. Creep crack initiation (defined as the first element reaching a damage level,  $\omega \approx 1.0$ ) is predicted to occur in the HAZ at the interface with the BM, as shown in Fig. 13a, after about 28,000 h. The results of the analysis also reveal that creep failure of the stubs-header weld connection occurs in the HAZ on the barrel side weld toe, Fig. 13b, which is consistent with the cracking location observed by the metallographic examinations on stubs weld shown in Fig. 13, for the service conditions (steam temperature 570 °C and internal pressure of 16.5 MPa). Although the FE analyses results correspond to the header operating in the ultra super-critical conditions, with a temperature higher than the realistic industrial service temperature, the industrial observations can still provide some useful insights regarding the damage behaviour of the header weldment and therefore could be used to qualitatively evaluate the capability of the FE predictions of the pressurised header. The failure time was considered as the time to achieve a damage level of around 1.0 in a small number of elements. It has been shown that the remaining creep time before complete failure occurs is relatively small compared to the total creep time [14,18]. The predicted creep crack growth

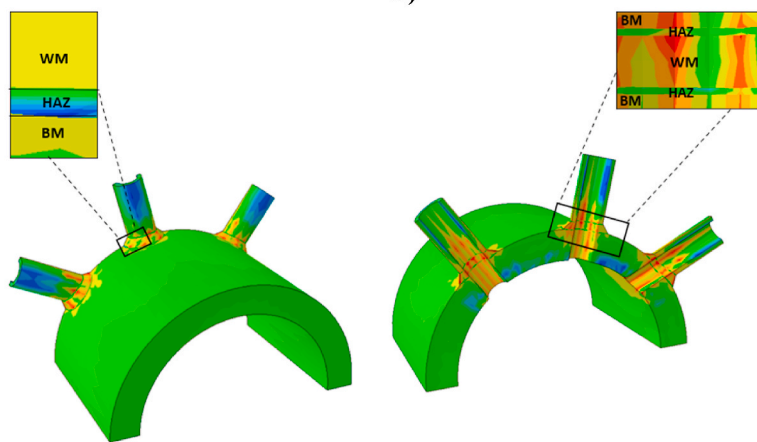
**Von Mises stress  
(MPa)**



a)



b)



c)

Fig. 12. Distributions of von Mises equivalent stress at a)  $t = 300$  h, b)  $t = 28,000$  h and c) at  $t \approx 40,000$  h (failure).

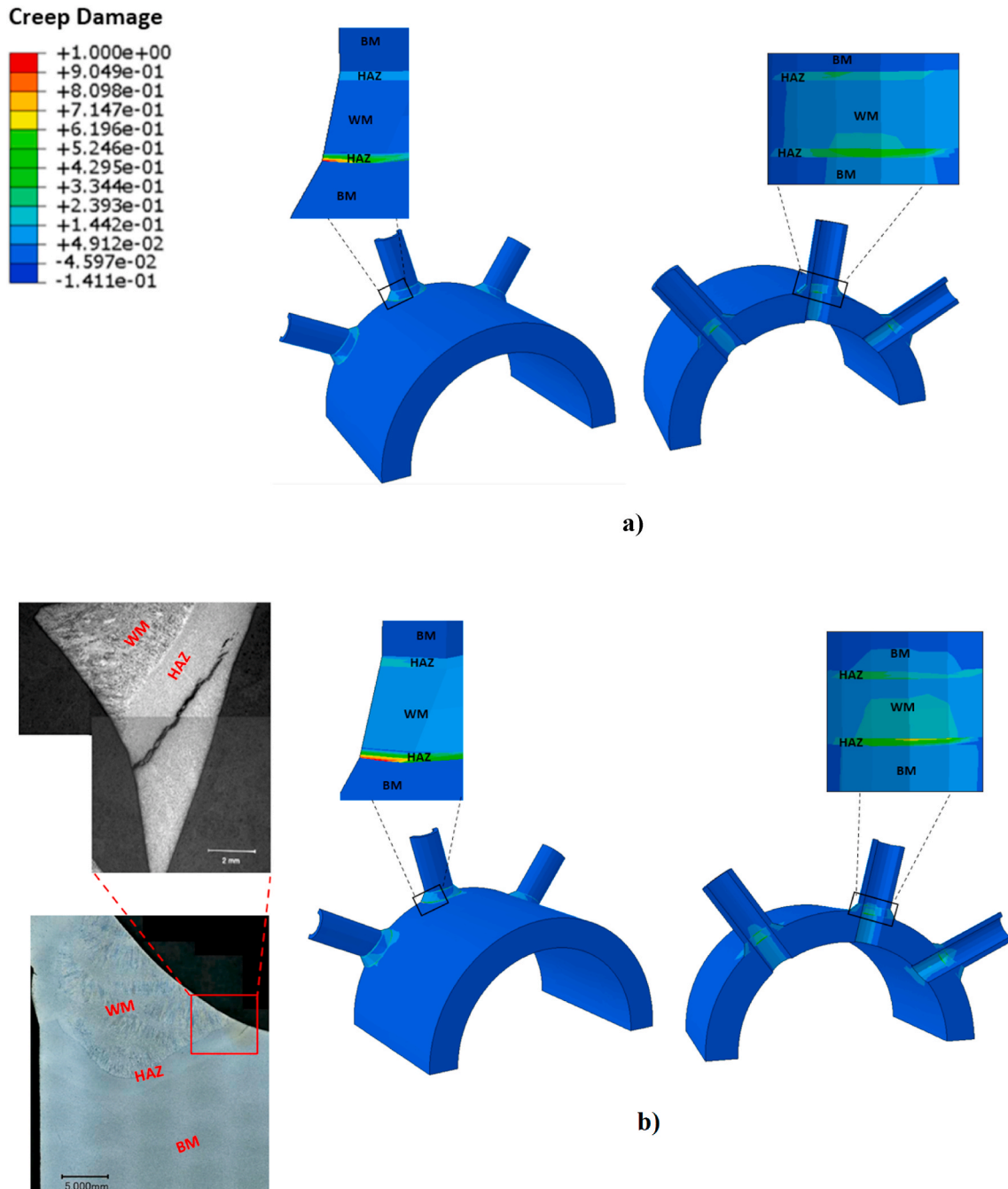


**Fig. 13.** Creep damage distribution and cracking for the stubs-header weld connection at a)  $t = 28,000$  h, and b) at failure ( $t \approx 40,000$  h) and the experimentally observed creep cracking on the stub-header weldment for the service conditions (steam temperature  $570$  °C and internal pressure of  $16.5$  MPa). (The experimental results are adapted from Ref. [32]).

behaviour is shown in Fig. 14a. As can be seen, crack starts to initiate after 70% of the total life had been consumed. Following crack initiation, Type IV cracking starts to propagate at increasing rates until the critical crack size is reached after around 40,000 h. The FE predictions of creep crack growth also indicate that close to failure the rate of crack propagation accelerates very quickly, leading to unstable crack growth. It should be noted that creep crack propagation results obtained in Fig. 14a is defined here as the critical damage growth path along the circumference on the outer surface of the stub tubes header-weld. In addition, the successive positions of the crack surface growth are presented for different creep times in Fig. 14a. To ensure the accuracy of the FE results, finer mesh with smaller element sizes has been applied locally in the HAZ region, as shown in Fig. 11b, where peak damage is expected

to occur. A prior mesh convergence study has been conducted, where creep crack growth predictions for different mesh sizes are obtained, as illustrated in Fig. 14b. To offer a compromise between the analysis costs and accuracy of FE results, a mesh density with an element size of 2 mm in the HAZ region is chosen, resulting in a small difference in the prediction of crack length (less than 2%) between the two finest meshes. It has been shown that a small difference in the convergence of creep crack growth could be acceptable (i.e., the numerical solutions can be considered to have converged) [37].

### 5. Conclusion and future work

In the present study, the creep-damage behaviour of a power plant

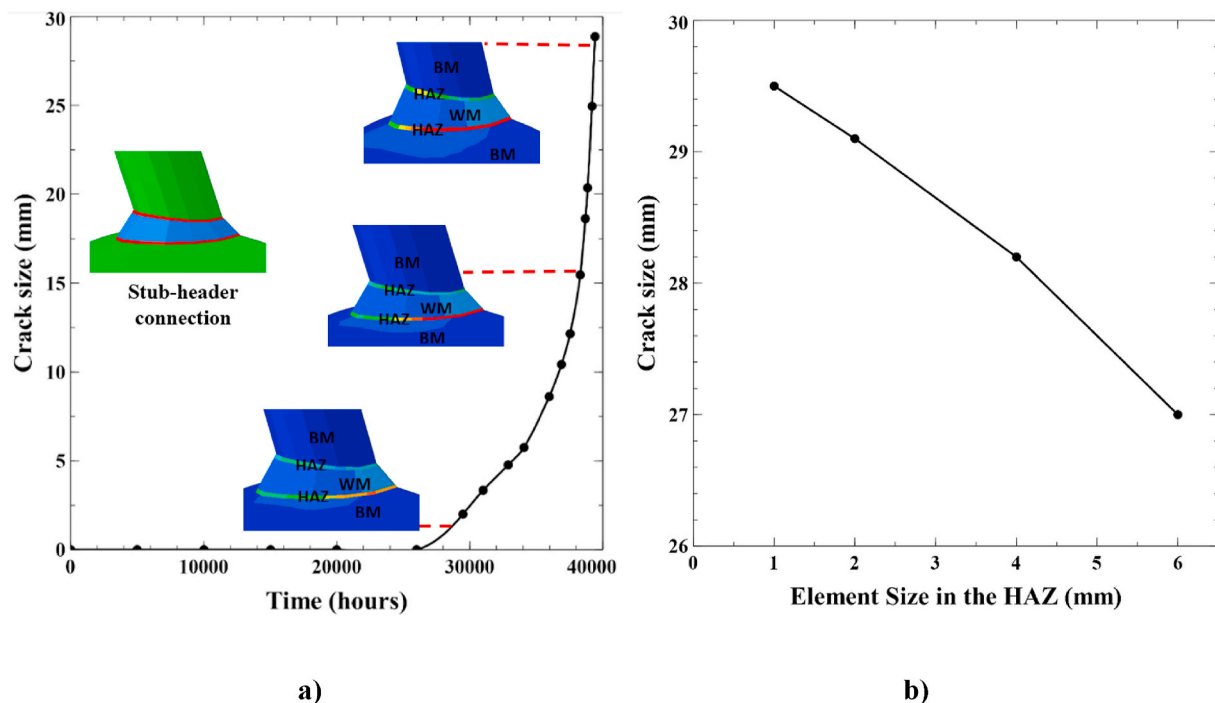


Fig. 14. a) FE prediction of circumferential creep crack growth on the outer surface of the stub tubes-header weld, b) Crack size vs. Element size in the HAZ (mesh sensitivity with respect to creep crack length).

pressurised header weldment operating under ultra super-critical conditions was investigated using a stress-based continuum mechanics model. The FE results have shown the capability of predicting expected failure location, compared to industrial observations. Following are some insights into future work:

1. Creep ductility effects on creep performance should be considered to account for the wide variability observed in the creep performance of CSEF steel cross-welds and therefore reduce the uncertainty when predicting long-term component performance. Besides, future models should offer the capability to evaluate the micro-damage in terms of the number densities of cavities, cavitation rate and cavity distributions for a specific alloy composition under given applied stress and temperature.
2. Creep damage constitutive laws need to be extended to account for the effects of stress state on creep deformation and damage in order to satisfy some other requirements, e.g., creep strain rate consistency and damage evolution consistency [9,38] and therefore produce more consistent results regarding lifetime and strain at failure for a wide range of stress state and stress level.
3. The methodology used to derive creep properties of the weldment could be improved in future work. This may involve utilization of miniature specimen testing and local hardness mapping to derive more accurate properties of the HAZ [39].

#### CRedit author contribution statement

Raheeg Ragab: Conceptualization, Methodology, Software, Formal analysis, Investigation, Data curation, Writing - original draft. Jonathan Parker: Conceptualization, Methodology, Writing - review & editing, Supervision. Ming Li: Conceptualization, Methodology, Writing - review & editing, Supervision. Tao Liu: Conceptualization, Methodology, Writing - review & editing, Supervision, Project administration, Funding acquisition. Wei Sun: Conceptualization, Methodology, Writing - review & editing, Supervision, Project administration, Funding acquisition.

#### Declaration of competing interest

The authors declare that they have no known competing financial interests or personal relationships that could have appeared to influence the work reported in this paper.

#### Acknowledgment

This work was supported by the Engineering and Physical Sciences Research Council (EPSRC). The funding is provided through the EPSRC Centre for Doctoral Training in Resilient Decarbonised Fuel Energy Systems (Grant number: EP/S022996/1). The work was also partly sponsored by the Biomass and Fossil Fuel Research Alliance (BF2RA). The authors would also like to acknowledge EPRI for the technical support, and for permission to use their experimental results and publish this paper.

#### References

- [1] R. Viswanathan, J.F. Henry, J. Tanzosh, G. Stanko, J. Shingledecker, B. Vitalis, et al., U.S. program on materials technology for ultra-supercritical coal power plants, *J. Mater. Eng. Perform.* 14 (3) (2005) 281–292, <https://doi.org/10.1361/10599490524039>.
- [2] F. Masuyama, *New developments in steels for power generation boilers*, in: *Advanced Heat Resistant Steel for Power Generation*, Institute of Materials, 1999, pp. 33–48.
- [3] S.J. Brett, D.L. Oates, C. Johnston, *In-service type IV cracking on a modified 9Cr (Grade 91) header*, in: *ECCC Conference: Creep & Fracture in High Temperature Components - Design & Life Assessment Issues*, IMechE, London, 2005, September 12–14, 2005.
- [4] J. Parker, S. Brett, *Creep performance of a Grade 91 header*, *Int. J. Pres. Ves. Pip.* 111–112 (2013) 82–88, <https://doi.org/10.1016/j.ijpvp.2013.05.003>.
- [5] L. Kachanov, *On Rupture Time under Condition of Creep*, vol. 8, *Izvestia Akademii Nauk USSR, Otd. Techn. Nauk, Moskva*, 1958, pp. 26–31.
- [6] Y. Liu, S. Murakami, *Damage localisation of conventional creep damage models and proposition of a new creep damage analysis*, *JSM Int. J. of Solid Mechanics & Material Engineering, Series A* 41 (1) (1998) 57–65, <https://doi.org/10.1299/jsmea.41.57>.
- [7] Z.L. Kowalewski, D.R. Hayhurst, B.F. Dyson, *Mechanisms-based creep constitutive equations for an aluminium alloy*, *J. Strain Anal. Eng. Des.* 29 (1994) 309–316, <https://doi.org/10.1243/03093247V294309>.

- [8] I. Perrin, D. Hayhurst, Creep constitutive equations for a 0.5 Cr–0.5 Mo–0.25 V ferritic steel in the temperature range 600–675°C, *J. Strain Anal. Eng. Des.* 31 (4) (1996) 299–314, <https://doi.org/10.1243/03093247V314299>.
- [9] Q. Xu, Creep damage constitutive equations for multi-axial states of stress for 0.5 Cr 0.5 Mo 0.25 V ferritic steel at 590 °C, *Theor. Appl. Fract. Mech.* 36 (2) (2001) 99–107, [https://doi.org/10.1016/S0167-8442\(01\)00060-X](https://doi.org/10.1016/S0167-8442(01)00060-X).
- [10] R.W. Evans, J.D. Parker, B. Wilshire, An extrapolative procedure for long term creep strain and creep life prediction with special reference to 0.5Cr0.5Mo0.25V ferritic steels, in: *Recent Advances in Creep and Fracture Engineering Materials and Structures*, Pineridge Press, Swansea, 1982, ISBN 0906674-18-2, pp. 135–184.
- [11] D.N. Robinson, R.W. Swindeman, Unified Creep-Plasticity Constitutive Equations for 2-1/4 Cr-1 Mo Steel at Elevated Temperature, 1982, <https://doi.org/10.2172/708802>. United States: N. p. Web.
- [12] F.R. Hall, D.R. Hayhurst, Continuum damage mechanics modelling of high temperature deformation and failure in a pipe weldment, *Proc. R. Soc.* 433 (1991) 383–403, <https://doi.org/10.1098/rspa.1991.0054>.
- [13] T.H. Hyde, W. Sun, Determining high temperature properties of weld materials, *JSME Int. J. of Solid Mechanics & Material Engineering, Series A* 43 (2000) 408–414, <https://doi.org/10.1299/jsmea.43.408>.
- [14] T.H. Hyde, W. Sun, A.A. Becker, J.A. Williams, Creep properties and failure assessment of new and fully repaired P91 pipe welds at 923 K, *Proc. Inst. Mech. Eng. Part L: J. Materials: Design and Applications* 218 (2004) 211–222, <https://doi.org/10.1177/146442070421800305>.
- [15] T.H. Hyde, A.A. Becker, W. Sun, J.A. Williams, Finite element creep damage analyses of P91 pipes, *Int. J. Pres. Ves. Pip.* 83 (2006) 853–863, <https://doi.org/10.1016/j.ijpvp.2006.08.013>.
- [16] D.R. Hayhurst, I.W. Goodall, R.J. Hayhurst, D.W. Dean, Lifetime prediction for high temperature low-alloy ferritic steel weldments, *J. Strain Anal. Eng. Des.* 40 (7) (2005) 675–701, <https://doi.org/10.1243/030932405X30885>.
- [17] R. Mustata, D.R. Hayhurst, F. Vakili-Tahami, CDM predictions of creep damage initiation and growth in ferritic steel weldments in a medium bore branched pipe under constant pressure at 590 °C using a 4 material weld model, *Arch. Appl. Mech.* 75 (2006) 475–495, <https://doi.org/10.1007/s00419-005-0423-4>.
- [18] T.H. Hyde, W. Sun, A.A. Becker, Creep crack growth in welds: a damage mechanics approach to predicting initiation and growth of circumferential cracks, *Int. J. Pres. Ves. Pip.* 78 (2001) 765–771, [https://doi.org/10.1016/S0308-0161\(01\)00088-6](https://doi.org/10.1016/S0308-0161(01)00088-6).
- [19] T.H. Hyde, J.A. Williams, A.A. Becker, W. Sun, The influence of heat affected zone characteristics on the creep failure of P91 welds: an initial sensitivity study using steady state creep, in: *Material Science Forum*, vols. 440–441, Trans Tech Publications, Switzerland, 2003, pp. 465–472, <https://doi.org/10.4028/www.scientific.net/MSF.440-441.465>.
- [20] T.H. Hyde, M. Saber, W. Sun, Creep crack growth data and prediction for a P91 weld at 650 °C, *Int. J. Pres. Ves. Pip.* 87 (2010) 721–729, <https://doi.org/10.1016/j.ijpvp.2010.09.002>.
- [21] M. Li, R.A. Barrett, S. Scully, N.M. Harrison, S.B. Leen, P.E. O'Donoghue, Cyclic plasticity of welded P91 material for simple and complex power plant connections, *Int. J. Fatig.* 87 (2016) 391–404, <https://doi.org/10.1016/j.ijfatigue.2016.02.005>.
- [22] V. Shlyannikov, A. Tumanov, Creep damage and stress intensity factor assessment for plane multi-axial and three-dimensional problems, *Int. J. Solid Struct.* 150 (2018) 166–183, <https://doi.org/10.1016/j.ijsolstr.2018.06.009>.
- [23] A.C.F. Cocks, M.F. Ashby, Intergranular fracture during power-law creep under multiaxial stresses, *Met. Sci.* 14 (8–9) (1980) 395–402, <https://doi.org/10.1179/030634580790441187>.
- [24] J.F. Wen, S.T. Tu, A multiaxial creep-damage model for creep crack growth considering cavity growth and microcrack interaction, *Eng. Fract. Mech.* 123 (2014) 197–210, <https://doi.org/10.1016/j.engfracmech.2014.03.001>.
- [25] N. Kim, C. Oh, Y. Kim, C. Davies, K. Nikbin, D. Dean, Creep failure simulations of 316H at 550°C: Part II – effects of specimen geometry and loading mode, *Eng. Fract. Mech.* 105 (2013) 169–181, <https://doi.org/10.1016/j.engfracmech.2013.04.001>.
- [26] V. Shlyannikov, A. Tumanov, Creep-fracture resistance parameters determination based on stress and ductility damage models, *Fatig. Fract. Eng. Mater. Struct.* 41 (2018) 2110–2129, <https://doi.org/10.1111/ffe.12766>.
- [27] T.H. Hyde, A.A. Becker, W. Sun, A. Yaghi, J.A. Williams, S. Concar, Determination of creep properties for P91 weldment materials at 625°C, in: *5th Int Conf on Mechanics and Materials in Design*. University of Porto, Portugal, 24–26 July 2006, 2006. <https://pdfs.semanticscholar.org/b426/9d1155515a7ee2c263a5cb3dec7228345e59.pdf>.
- [28] M. Saber, D. Tanner, W. Sun, T.H. Hyde, Determination of creep and damage properties for P92 at 675°C, *J. Strain Anal. Eng. Des.* 46 (2011) 842–851, <https://doi.org/10.1177/0309324711413012>.
- [29] ABAQUS 2019 Online Documentation, 2019 (© Dassault Systèmes).
- [30] J.A. Siefert, The Influence of the Parent Metal Condition on the Cross-Weld Creep Performance in Grade 91 Steel, PhD thesis, Loughborough University, 2019, <https://doi.org/10.26174/thes.lboro.8309882.v1>. Available on.
- [31] J. Siefert, J. Parker, R. MacLachlan, S. Yan, R. Thomson, Assessment and quantification of damage in the Grade 91 steel partially transformed zone, in: *Conference Contribution*, Loughborough University, 2019. <https://hdl.handle.net/2134/12443297.v1>.
- [32] *Review of Fabrication and In-Service Performance of a Grade 91 Header*, EPRI, Palo Alto, CA, 2013, p. 3002001831.
- [33] D.R. Hayhurst, “Creep rupture under multi-axial states of stress”, *J. Mech. Phys. Solid.* 20 (1972) 381–390, [https://doi.org/10.1016/0022-5096\(72\)90015-4](https://doi.org/10.1016/0022-5096(72)90015-4).
- [34] J. Parker, J. Siefert, Manufacture and performance of welds in creep strength enhanced ferritic steels, *Materials* 12 (2019) 2257, <https://doi.org/10.3390/ma12142257>.
- [35] Y. Takahashi, H. Shigeyama, J. Siefert, J. Parker, Effect of simulated heat affected zone thermal cycle on the creep deformation and damage response of Grade 91 steel including heat-to-heat variation, in: *Proceedings of the ASME 2018 Pressure Vessels and Piping Conference*, July 15–20, 2018, Prague, Czech Republic, 2018, <https://doi.org/10.1115/PVP2018-85102>.
- [36] Y. Takahashi, H. Shigeyama, J. Siefert, J. Parker, A summary of 10 years research on Grade 91 and Grade 92 steel, in: *International Conference on Advances in High Temperature Materials*, Nagasaki (Japan), October 21–24, 2019, 2019.
- [37] C.J. Hyde, T.H. Hyde, W. Sun, A.A. Becker, Damage mechanics-based predictions of creep crack growth in 316 stainless steel, *Eng. Fract. Mech.* 77 (12) (2010) 2385–2402, <https://doi.org/10.1016/j.engfracmech.2010.06.011>.
- [38] Q. Xu, S. Barrans, The development of multiaxial creep damage constitutive equations for 0.5Cr-0.5Mo-0.25 V ferritic steel at 590° C, *JSME Int. J.* 46 (1) (2003) 51–59, <https://doi.org/10.1299/jsmea.46.51>.
- [39] W. Wen, W. Sun, A.A. Becker, A two-material miniature specimen test method and the associated inverse approach for high temperature applications, *Theor. Appl. Fract. Mech.* 99 (1–8) (2019), <https://doi.org/10.1016/j.tafmec.2018.10.008>.